

Femtosecond laser electronic excitation tagging applied to velocity measurement in hypersonic boundary layer flows

Yuhong Deng^{a,b}, Zhengyue Qu^a, Shicheng Tang^a, Xilong Yu^{a,b*}, Shaohua Zhang^a, Xin Lin^{a,b}, Qiu Wang^a, Wei Zhao^{a,b}

^aKey Laboratory of High Temperature Gas Dynamics, Institute of Mechanics, CAS, No.15 Beisihuanxi Road, Beijing, China 100190; ^bUniversity of Chinese Academy of Sciences, Beijing, China 100049

ABSTRACT

The flight process of hypersonic vehicles involves complex flow interactions, such as boundary layer transition and shock-wave/boundary-layer interactions, making velocity measurement within the boundary layer crucial for understanding aerodynamic characteristics. Femtosecond Laser Electronic Excitation Tagging (FLEET) offers significant advantages over traditional Molecular Tagging Velocimetry (MTV) by measuring hypersonic flows without the need for tracer particles. However, measuring velocity within the boundary layer remains challenging due to near-wall effects and flow disturbances. This study investigates the applicability of FLEET in hypersonic boundary layer flows, aiming to enhance understanding of boundary layer characteristics and provide data for numerical simulations. The JF10 wind tunnel generates high-temperature and high-pressure gases by detonating a hydrogen-oxygen mixture, producing a shockwave that compresses nitrogen test gas. The gas is then expanded through a nozzle to create a hypersonic flow field. A femtosecond laser focuses near the surface of a blunt-cone model, and an intensified ICCD camera captures the measurements. Velocity profiles were obtained under $Ma=8.9$ inflow conditions, considering factors like femtosecond filament imaging resolution. The results show that FLEET is effective for velocity measurement in the hypersonic boundary layer, with fitting coefficients exceeding 99.2%. The measurement uncertainty was determined to be 12.4%. The results validate FLEET as a feasible technique for velocity measurements in hypersonic boundary layer flows, and future research will integrate it with other laser diagnostic techniques for improved accuracy.

Keywords: femtosecond laser, filament, molecular tagging, high-enthalpy wind tunnel, velocity measurement, boundary layer

1. INTRODUCTION

During the flight of hypersonic vehicles, complex flow phenomena within the boundary layer significantly influence their performance and fuel efficiency. A deeper understanding of the boundary layer flow process is critical for the design and development of hypersonic vehicles^[1]. Existing turbulence models^[2-4] for boundary layers are inadequate for predicting flow behavior under hypersonic conditions due to the complexities introduced by high-temperature effects, laminar-turbulent transition, and shock wave-boundary layer interactions. Accurate theoretical predictions and improvements to these models depend heavily on high-quality experimental data from ground-based facilities, such as wind tunnels.

Velocity is one of the most important parameters in characterizing the flow field. In wind tunnel experiments, velocity measurement techniques for gas flow fields are generally categorized into contact and non-contact methods. Traditional contact methods, such as Pitot tubes^[5] and hot-wire anemometry^[6], involve inserting probes into the flow field, which can cause significant disturbances—such as shock waves—that interfere with the flow and reduce the accuracy of measurements, especially in hypersonic flows. Non-contact methods greatly minimize such disturbances. With advances in laser technology, non-contact methods such as Particle Imaging Velocimetry^[7] (PIV) and Laser Doppler Velocimetry^[8] (LDV) have been widely adopted for velocity measurements. However, these techniques typically require the addition of

*Corresponding author e-mail address: xlyu@imech.ac.cn

micron- or nanometer-scale solid or liquid tracer particles, which may fail to accurately follow rapid velocity changes in near-wall regions or shock layers, leading to significant measurement errors. Molecular Tagging Velocimetry^[9] (MTV), which uses well-following molecules as tracers, has addressed the issue of poor particle tracking and has been instrumental in hypersonic flow measurements. However, traditional MTV systems often suffer from high complexity and limited applicability.

Recent techniques, such as Raman Excitation Plus Laser-Induced Fluorescence^[10] (RELIEF) and Femtosecond Laser Electronic Excitation Tagging^[11-14] (FLEET), utilize nitrogen as a tracer without the need for additional seeding molecules, thus significantly simplifying the setup requirements for conventional MTV. This study focuses on FLEET technology, which was first proposed by Michael et al^[13]. from Princeton University in 2011. They used nitrogen tracers to achieve point velocity measurements in nitrogen jet flows and subsequently applied this technique to the study of combustion^[15], subsonic^[16], supersonic^[17], and hypersonic flows^[18,19]. Although FLEET has been shown to be a feasible method for free-stream velocity characterization, challenges remain in measuring velocity in hypersonic boundary layers due to near-wall effects and flow disturbances^[20]. In this research, the FLEET technique is implemented on the JF10 hydrogen-oxygen detonation-driven shock tunnel platform to measure the velocity distribution within the boundary layer of a blunt-cone model. The experimental setup, utilizing an ICCD camera with dual shutters, captures the velocity field under Mach 8.9 conditions, with nitrogen gas used to mitigate fluorescence quenching effects^[21]. The velocity data obtained will provide valuable insights into hypersonic boundary layer characteristics, including velocity distribution, turbulence properties, and potential separation phenomena. These measurements will serve as a reference for numerical simulations and contribute to the performance evaluation and improvement of hypersonic vehicles, missiles, and other aerodynamic systems.

2. EXPERIMENTAL PRINCIPLES

When high-power ultrafast lasers propagate through transparent media, if the power of the femtosecond laser exceeds the self-focusing threshold P_{cr} , a dynamic balance between the defocusing effect of the plasma and the focusing effect of the Kerr effect will occur due to the interplay of nonlinear and linear effects. This process creates a plasma channel, known as a "filament," and the phenomenon is referred to as femtosecond laser filamentation^[22]. Another notable feature of this filamentation process is the significant broadening of the laser spectrum, covering a range from microwaves to ultraviolet. The critical power threshold for filamentation is given by:

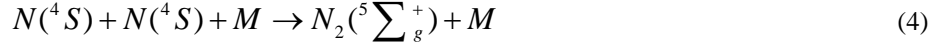
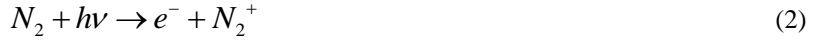
$$P_{cr} = \frac{3.72\lambda_0^2}{8\pi n_0 n_2} \quad (1)$$

where λ_0 is the laser wavelength in vacuum, and n_0 and n_2 are the linear and nonlinear refractive indices of the medium, respectively. In atmospheric conditions, the electron density within the plasma channel formed by the femtosecond laser reaches $10^{16}\sim 10^{18}\text{cm}^{-3}$, with a typical filament radius of about $100\mu\text{m}$. The power density inside the filament is stable around 10^{14}W/cm^2 , which is sufficient to excite nitrogen molecules in the flow field from their ground state to excited energy levels through processes such as collision, energy transfer, and laser-induced photochemical reactions. The excited molecules then return to lower energy states, emitting fluorescence.



Figure 1. Filamentation of 800 nm femtosecond laser in air (laser energy: 400mJ, EVs: 20s)

Figure 2 illustrates the energy level transitions of nitrogen molecules through laser-induced dissociation. Nitrogen primarily undergoes tunnel ionization, forming N_2^+ and electrons. The following key processes are involved in the excitation and recombination of nitrogen molecules^[23]:



The transitions from $N_2(B-A)$, $N_2(C-B)$ and $N_2^+(B-X)$ correspond to the First Positive System (FPS, 500-900 nm), Second Positive System (SPS, 320-410 nm), and First Negative System (FNS, 320-500 nm), respectively. In pure nitrogen, the fluorescence lifetimes of the FNS and SPS signals are approximately 50ns, while the FPS signal can persist for tens of microseconds, depending on vibrational relaxation processes. By capturing the displacement of excited molecules using a dual-shutter ICCD camera, the velocity information of the flow field can be obtained.

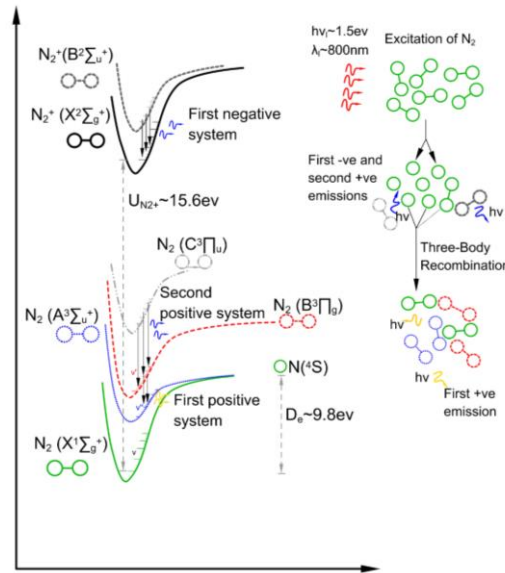


Figure 2. Energy level diagram of nitrogen molecules in FLEET system^[24].

3. EXPERIMENTAL SETUP

The experimental setup for FLEET measurements is illustrated in Figure 3. The system comprises the JF10 hydrogen-oxygen detonation-driven shock wind tunnel, a blunt-cone model, a femtosecond laser, an optical system, a dual-shutter ICCD (PI MAX4), a delay controller (DG645), and an oscilloscope. The JF10 shock wind tunnel features quartz optical windows on both sides and the top of the test section, allowing optical access for measurements in the near-infrared range. The femtosecond laser is focused by a convex lens (focal length 1000mm) near the surface of the blunt-cone model. The ICCD camera is positioned above the test section, capturing the flow field through the top quartz window.

The timing of the experiment is controlled by the DG645 delay generator, which synchronizes the laser pulse and camera trigger with nanosecond precision.

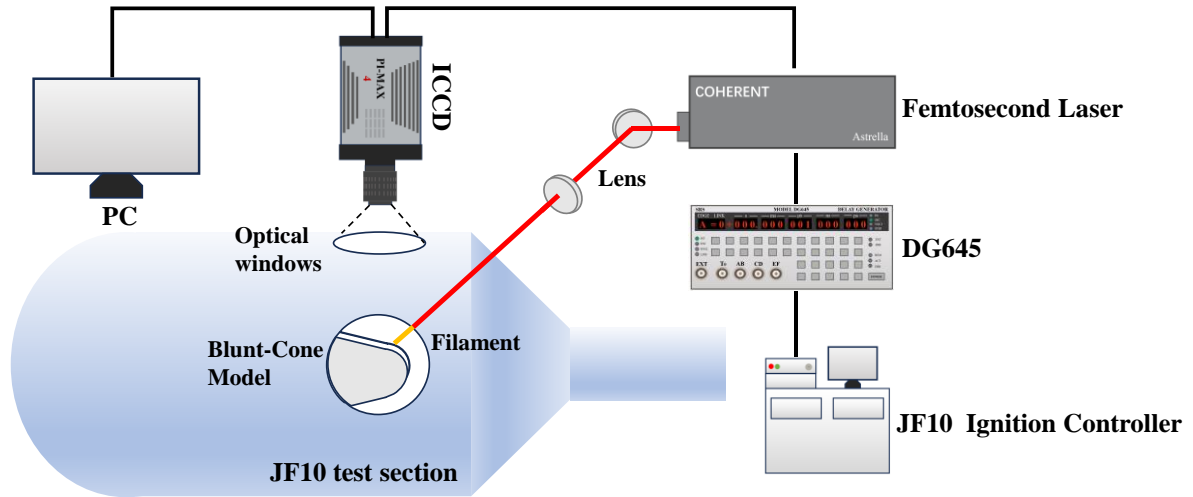


Figure 3. Schematic diagram of the FLEET experimental system.

3.1 JF10 Wind Tunnel

Figure 4 shows a schematic diagram of the JF10 hydrogen-oxygen detonation-driven shock wind tunnel. The tunnel, approximately 40 meters in length, consists of a detonation-driven section, an expansion section, a driven section, a nozzle, a test section, a vacuum chamber, and a vacuum pump. The high-temperature (above 3000 K) and high-pressure (peak pressure up to 30 MPa) gas generated by the detonation of hydrogen and oxygen drives strong shock waves in the driven section.

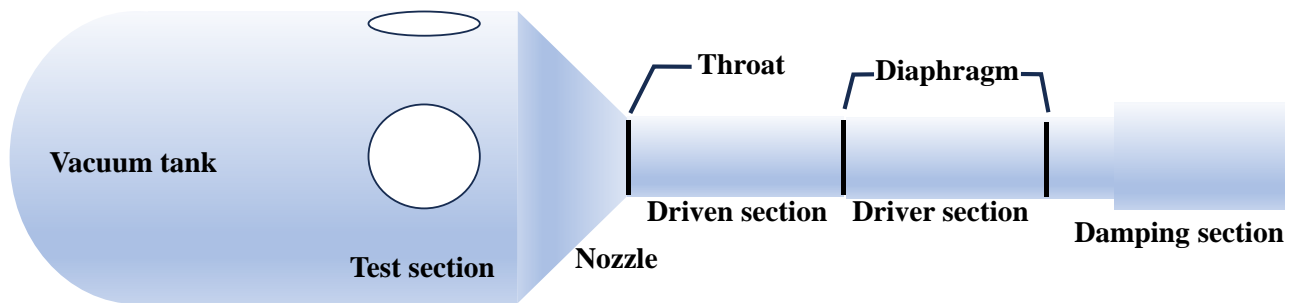


Figure 4. Schematic diagram of the JF10 hydrogen-oxygen detonation-driven shock wind tunnel

Since its construction in 1998, the JF10 tunnel has undergone several upgrades and currently operates in a forward detonation mode^[25]. In the FLEET experiments, the driven section is filled with nitrogen gas at 8kPa, while the detonation section is filled with a 2:1 hydrogen-oxygen mixture at 1.5MPa. The compressed nitrogen gas generates high-enthalpy and high-Reynolds-number flows, forming a hypersonic flow field upon expansion through the nozzle^[26]. The operational parameters of the tunnel are detailed in Table 1.

Table 1. JF10 wind tunnel operation status

Initial conditions			Stagnation conditions				Nozzle exit parameters	
H ₂ :O ₂	P _{4i} (MPa)	P ₁ (kPa)	P ₀₅ (MPa)	T ₀₅ (K)	H ₀ (MJ/kg)	M _s	M _e	
2:1	1.5	8	7.1	6100	11.3	5.2	8.9	

3.2 Blunt-Cone Model

The blunt-cone model used in this experiment was mounted and secured through a downstream support strut, connected to a base support. The model has a blunt nose with a radius of 50mm, a half-angle of 8° , and a total length of 300mm. Figure 5 shows the physical structure of the blunt-cone model, which indicates the locations of two measurement points. These points are positioned at the center of the side surface, located 200mm and 100mm from the model's nose.

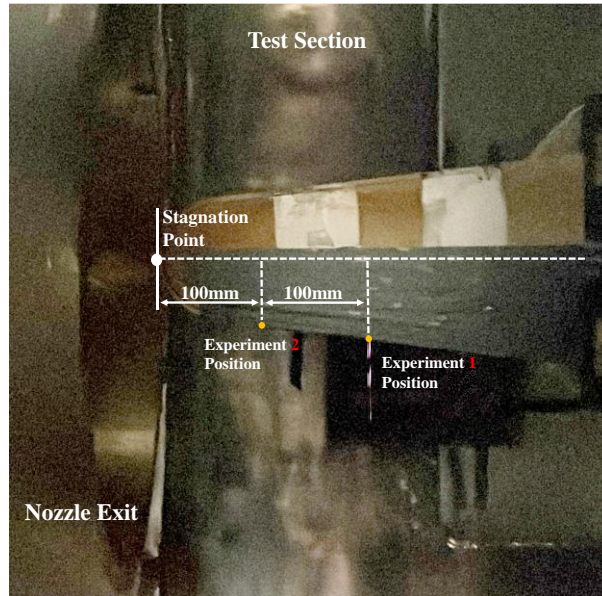


Figure 5. Physical structure of the blunt-cone model.

3.3 Optical Diagnostics

A Ti:sapphire femtosecond laser (Coherent Astrella USP) served as the excitation source for molecular nitrogen multiphoton dissociation in this experiment. The laser generated femtosecond pulses with a central wavelength of 800 nm, pulse width of approximately 35fs, and a maximum repetition rate of 1kHz. The laser beam, with a diameter of approximately 10mm, was operated at a repetition rate of 1kHz for all experimental conditions. The pulse energy was set at 3mJ, and the laser wavelength was 800nm, controlled via the Revolution pump source, with energy output monitored using a power meter.

The optical system was comprised of a femtosecond laser, a beam lift system, mirrors, a variable aperture diaphragm, a 1000mm focal length convex lens, and laser beam blockers. The beam lift system raised the femtosecond laser to the same horizontal level as the center of the blunt-cone model within the test section of the JF10 wind tunnel. The adjustable diaphragm had a maximum diameter of 12mm, and the 1000mm convex lens focused the laser beam approximately 9mm from the side surface center of the blunt-cone model.

For fluorescence detection, a high-resolution, dual-shutter ICCD camera (PI-MAX4:1024i) was employed, capable of achieving a minimum gate width of 3ns and a minimum delay between frames of 1060 ns. The camera sensor had a pixel size of $12.8\mu\text{m}$, allowing for high time-resolution imaging.

Timing control is critical for the accurate FLEET velocity measurements in the JF10 wind tunnel. The JF10 operates in a pulse mode, with an optimal test duration of approximately 4ms, while the femtosecond laser generates one pulse per millisecond at its 1kHz repetition rate. The nitrogen fluorescence lifetime induced by the femtosecond laser filament lasts on the order of microseconds, and the ICCD camera gate width is controlled within the range of hundreds of nanoseconds. Timing precision for the entire experiment is achieved using the DG645 delay generator, with a root-mean-square jitter of less than 25ps for output signals. Since there is a periodic jitter of laser pulses within each millisecond, fluorescence signal collection is triggered directly by the femtosecond laser control system with a jitter of less than 100ps.

In this experiment, the laser output occurred 7.5ms after the detonation of the JF10 shock wind tunnel, while the ICCD camera began capturing fluorescence signals at approximately 10.5ms. The ICCD camera's dual-shutter settings are shown in Table 2.

Table 2. ICCD camera's dual-shutter settings

Parameter	Value
Gain (%)	40-60
Delay 1 (ns)	10
Gate Width 1 (ns)	40
Delay 2 (ns)	1100
Gate Width 2 (ns)	100-500

The timing diagram of the primary FLEET measurement equipment is shown in Figure 6.

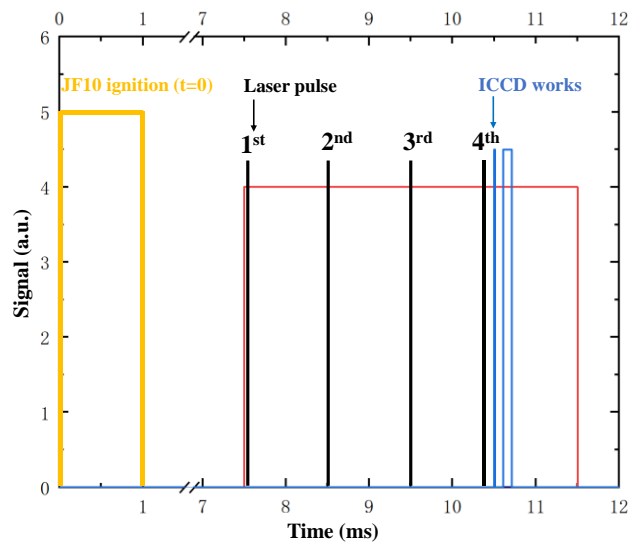


Figure 6. The timing control of the FLEET measurement system

4. EXPERIMENTAL RESULTS AND ANALYSIS

4.1 FLEET Experimental Results

Figure 7 shows the experimental results captured by the dual-shutter ICCD camera through the top quartz window of the JF10 wind tunnel test section. In Figure 7(left), the region corresponding to the laser filament exhibits significantly higher fluorescence intensity compared to the sum of aerodynamic heating and thermal radiation near the blunt-cone model, appearing as a bright line. This "bright line" represents the location of the femtosecond laser-induced fluorescence. The black region in the upper part of the image corresponds to the boundary of the blunt-cone model, which has a half-angle of 8°. Figure 7(right) shows the image captured 1100ns after the initial exposure. The measurement was taken at the center of the side surface, located 200mm from the stagnation point.

Due to the relatively short fluorescence lifetimes associated with nitrogen's first negative system $N_2^+(B-X)$ and second positive system $N_2(C-B)$, the fluorescence intensity in the delayed image is considerably weaker than that of the initial exposure. Consequently, the laser filament appears as a "dark line" in the second frame. Similar "dark line" images have

been observed in previous FLEET velocity measurements conducted by Dogariu^[27] under Mach 10 conditions in the AEDC Tunnel 9.

The intense self-emission near the blunt-cone model is mainly attributed to phenomena such as high-temperature excitation and ionization radiation, aerodynamic heating, and thermal radiation. The varying gate widths between the two frames, as indicated in Table 2, account for the differing intensities of self-emission captured in the images. By analyzing the fluorescence intensity in regions far from the laser filament, it was determined that the variation in intensity remained below 3%, indicating that blackbody radiation and long-lived fluorescence primarily contributed to the self-emission intensity.

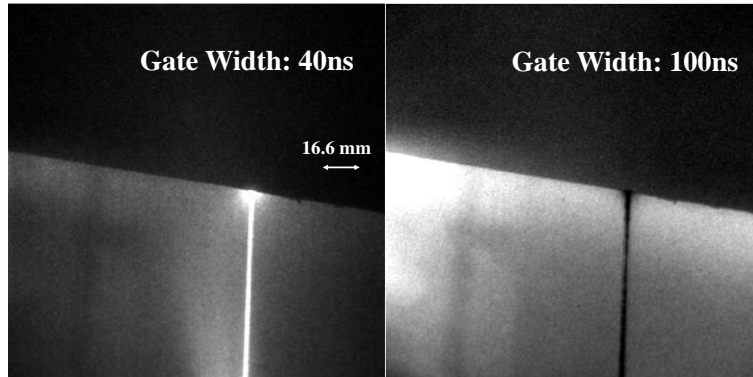


Figure 7. Femtosecond laser-induced fluorescence images on JF10 platform before (left) and after (right) a specific time delay

4.2 Data Processing and Analysis

A pixel-by-pixel calibration was conducted to convert the raw image data into physical distances. As shown in Figure 8, calibration was performed using a reference scale in both the horizontal and vertical directions near the region of interest. The conversion factor for this setup was determined to be 1 pixel corresponding to 1/6mm of real distance. The magnification of the camera system was thus calculated as approximately 1:13 based on the sensor size and the actual distance.

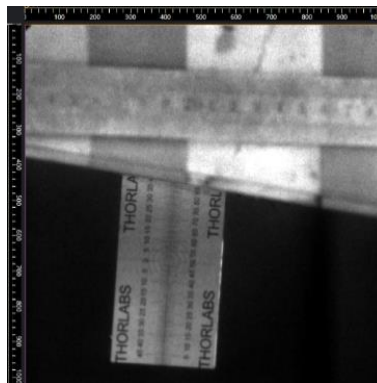


Figure 8. Pixel calibration for raw image data

The data processing procedure for the femtosecond laser filament-induced fluorescence images is illustrated in Figure 9. To process the data, the raw grayscale image was converted into a coordinate system where the upper-left corner of the image (0,0) served as the origin. First, the boundary of the blunt-cone model was identified using an edge detection algorithm based on the Canny operator. Given that the side boundary of the blunt-cone can be approximated as a linear boundary, the detected boundary was further refined through linear fitting. The standard deviation of the slope σ_k and intercept σ_b of the linear fit were calculated to be better than 0.001 and 0.05, respectively.

The fluorescence intensity profile of the laser filament was fitted using a Voigt function, which accounts for both Gaussian and Lorentzian broadening due to the actual gas pressure and instrument response:

$$y = y_0 + A \left[\mu \frac{2}{\pi} \frac{\omega}{4(x-x_c)^2 + \omega^2} + (1-\mu) \frac{\sqrt{4\ln 2}}{\sqrt{\pi}\omega} e^{-\frac{4\ln 2}{\omega^2}(x-x_c)^2} \right] \quad (9)$$

where x_c is the center position, A is the amplitude, ω is the full width at half maximum (FWHM), and μ is the shape factor.

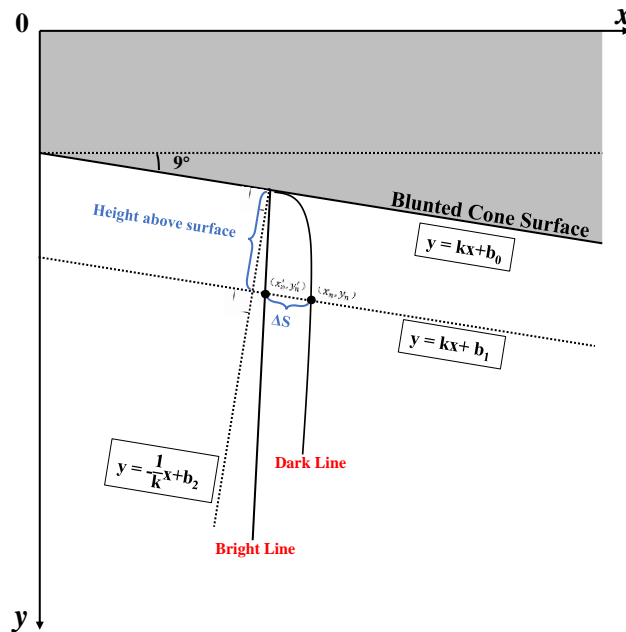


Figure 9. Schematic of the data processing procedure for fluorescence images

The fitting results for the fluorescence intensity profiles of the "bright line" and "dark line" are shown in Figure 10. The goodness of fit, represented by R^2 , was greater than 99.2% for all measurements. The center positions and FWHM of the laser filament before and after displacement were extracted with standard errors of less than 0.05 pixels. The average FWHM of the laser filament before displacement was 7.87 pixels, and after displacement, it increased to 12.69 pixels.

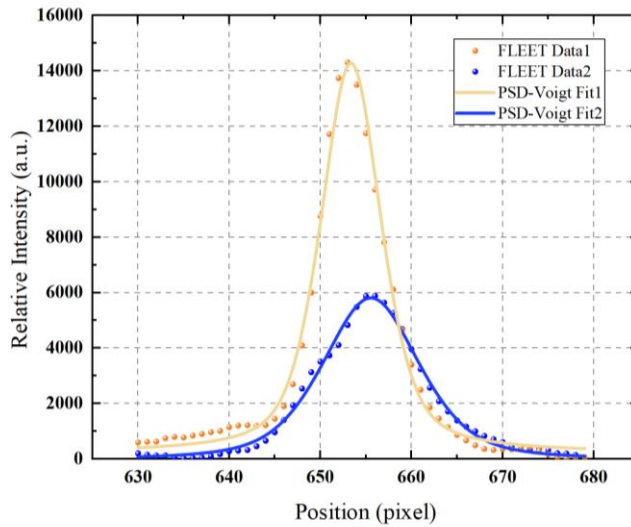


Figure 10. Voigt function fitting results for the fluorescence intensity distribution of the laser filament

By fitting the fluorescence intensity of the "bright line," the coordinates of the filament's emission point at the blunt-cone surface were determined. A normal line was then constructed perpendicular to the blunt-cone surface at this emission point, and the boundary layer height was defined as the distance along this normal direction. The displacement of the laser filament ΔS_n at different positions along the wall-normal direction was calculated as follows:

$$\Delta S_n = \sqrt{(x_n - x_n')^2 + (y_n - y_n')^2} \quad (10)$$

where (x_n, y_n) and (x_n', y_n') represent the positions of the "bright line" and "dark line" in the image, respectively, at different boundary layer heights. As both lines lie along lines parallel to the blunt-cone surface, the displacement can also be expressed as:

$$\Delta S_n = \sqrt{1 + k^2} |x_n - x_n'| \quad (11)$$

where k is the slope of the linear fit to the blunt-cone boundary.

The time interval Δt between the two images was controlled by the ICCD camera and was set to $\Delta t = t_i - t_j$ (ms). Using this time interval, the time-averaged FLEET velocity V_n at various positions along the wall-normal boundary layer height was calculated as:

$$V_n = \beta \frac{\Delta S}{\Delta t} \quad (12)$$

where β is the spatial scaling factor, converting pixel distances to millimeters (mm/pixel). The final FLEET velocity results for the two measurement points located 200mm and 100mm from the nose of the blunt-cone model are presented in Figure 11.

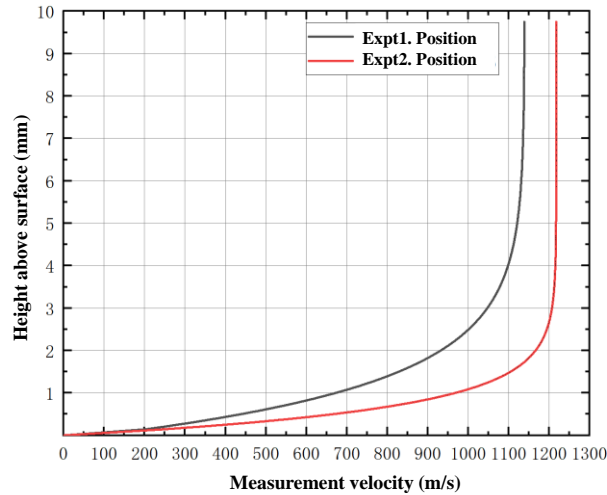


Figure 11. FLEET velocity measurement results at different boundary layer measurement positions

4.3 Uncertainty Analysis in Velocity Measurement

The uncertainty in velocity measurement stems from several factors, including the flow conditions in the high-enthalpy wind tunnel, the configuration of the FLEET system, and the data processing methods employed. Assuming that each direct measurement variable x_i introduces uncorrelated uncertainty, the combined standard uncertainty for velocity can be estimated using the error propagation formula:

$$u_V = \sqrt{\sum_{i=1}^N \left(\frac{\delta f}{\delta x_i}\right)^2 u_{x_i}^2} \quad (13)$$

where f represents the velocity function and u_{x_i} is the standard uncertainty in the direct measurement variable x_i .

The relative uncertainty in velocity E_V is given by:

$$E_V = \sqrt{\left(\frac{ku_k}{1+k^2}\right)^2 + \left(\frac{u_{x_n-x_n'}}{x_n-x_n'}\right)^2 + \left(\frac{u_\beta}{\beta}\right)^2 + \left(\frac{u_{\Delta t}}{\Delta t}\right)^2} \quad (14)$$

In this experiment, the fitted slope $k=0.16$ for the blunt-cone boundary, with a standard uncertainty of $u_k=0.003$. The uncertainty in the displacement measurement $|x_n-x_n'|$ is primarily determined by the standard error (SE) from the PSD-Voigt fit for the center position of the laser filament. Given that displacement greater than 10 times the SE (0.5 pixels) remains accurate, the uncertainty for displacement was estimated to be approximately 1%. The spatial scaling factor β was determined to be 0.167 mm/pixel, and the uncertainty in β arises from the calibration process of the image pixels. The A-type uncertainty from repeated calibration readings and the B-type uncertainty from the resolution limits yielded a total uncertainty in β of 0.011 pixels. For the time interval Δt , which was set to 1060ns, the combined uncertainty was calculated to be $u_{\Delta t}=5.7 \times 10^{-10}$ ms.

Finally, the relative uncertainty in the velocity measurement was determined to be:

$$E_V = \sqrt{(0.022)^2 + (0.01)^2 + (0.07)^2 + (5.4 \times 10^{-7})^2} = 12.4\% \quad (14)$$

The resolution of the FLEET velocity measurement system is limited by the pixel resolution of the ICCD camera and the magnification of the lens. By employing bilinear interpolation and fitting techniques, sub-pixel resolution was achieved, with an estimated velocity resolution $\Delta V=15.7$ m/s. Future work could further improve velocity resolution by enhancing the camera's magnification and optimizing image fitting algorithms.

5. CONCLUSION

In this study, we established a FLEET velocity measurement system using a femtosecond laser and a dual-shutter ICCD camera to measure the velocity distribution in the boundary layer of a blunt-cone model under hypersonic conditions. The experiments were conducted on the JF10 hydrogen-oxygen detonation-driven high-enthalpy shock wind tunnel platform, with velocity measurements obtained under Mach 8.9 flow conditions. The boundary layer velocity profiles at distances of 100mm and 200mm from the model's stagnation point were successfully captured, and the sources of measurement uncertainty were analyzed in detail. These results confirm the feasibility of using the FLEET system for complex flow measurements in hypersonic boundary layers. In the future, the FLEET diagnostic system will be integrated with other laser diagnostics, such as Schlieren interferometry and Doppler velocimetry, for simultaneous measurements at the same test locations to further enhance measurement accuracy and reliability.

ACKNOWLEDGEMENTS

This research is supported by the National Key R&D Program of China under the project "Development of High-Precision Propulsion Calibration Systems and Performance Testing Technologies" (Grant No. 2021YFC2202800).

REFERENCES

- [1] Anderson, J. D., [Hypersonic and high-temperature gas dynamics], American Institute of Aeronautics and Astronautics, Reston Va. (2006).
- [2] Liou, W. W., Huang, G. and Shih, T.-H., "Turbulence model assessment for shock wave/turbulent boundary-layer interaction in transonic and supersonic flows," *Computers & Fluids* 29(3), 275–299 (2000).
- [3] SAFFMAN, P. G. and WILCOX, D. C., "Turbulence-Model Predictions for Turbulent Boundary Layers," *AIAA Journal* 12(4), 541–546 (1974).
- [4] Parente, A., Górlé, C., van Beeck, J. and Benocci, C., "A Comprehensive Modelling Approach for the Neutral Atmospheric Boundary Layer: Consistent Inflow Conditions, Wall Function and Turbulence Model," *Boundary-Layer Meteorol* 140(3), 411–428 (2011).

- [5] Bailey, S. C. C., Hultmark, M., Monty, J. P., Alfredsson, P. H., Chong, M. S., Duncan, R. D., Fransson, J. H. M., Hutchins, N., Marusic, I., McKeon, B. J., Nagib, H. M., Örlü, R., Segalini, A., Smits, A. J. and Vinuesa, R., "Obtaining accurate mean velocity measurements in high Reynolds number turbulent boundary layers using Pitot tubes," *J. Fluid Mech.* 715, 642–670 (2013).
- [6] KOVASZNAY, L. S. G., "The Hot-Wire Anemometer in Supersonic Flow," *Journal of the Aeronautical Sciences* 17(9), 565–572 (1950).
- [7] Adrian, R. J., "Twenty years of particle image velocimetry," *Exp Fluids* 39(2), 159–169 (2005).
- [8] George, W. K. and Lumley, J. L., "The laser-Doppler velocimeter and its application to the measurement of turbulence," *Journal of Fluid Mechanics* 60(2), 321–362 (1973).
- [9] Koochesfahani, M., "Molecular Tagging Velocimetry (MTV) - Progress and applications," (06281999).
- [10] Webster, M. and Lempert, W., "Simplification of RELIEF Velocimetry Using Picosecond Tagging and Broad Band Interrogation," (01072008).
- [11] Fisher, J. M., Smyser, M. E., Slipchenko, M. N., Roy, S. and Meyer, T. R., "Burst-mode femtosecond laser electronic excitation tagging for kHz–MHz seedless velocimetry," *Opt. Lett.* 45(2), 335 (2020).
- [12] Zhang, Y., Marshall, G., Beresh, S. J., Richardson, D. and Casper, K. M., "Multi-line FLEET by imaging periodic masks," *Optics letters* 45(14), 3949–3952 (2020).
- [13] Michael, J. B., Edwards, M. R., Dogariu, A. and Miles, R. B., "Femtosecond laser electronic excitation tagging for quantitative velocity imaging in air," *Applied optics* 50(26), 5158–5162 (2011).
- [14] DeLuca, N. J., Miles, R. B., Kulatilaka, W. D., Jiang, N. and Gord, J. R., "Femtosecond Laser Electronic Excitation Tagging (FLEET) Fundamental Pulse Energy and Spectral Response," (2014).
- [15] Li, S. Y., Zhang, D. Y., Gao, Q., Li, B., He, Y. and Wang, Z. H., "Temperature Measurement of Combustion Fields Based on Femtosecond Laser Streak Imaging," *Acta Physica Sinica* 69(23), 168–174 (2020).
- [16] Burns, R. A., Danehy, P. M., Halls, B. R. and Jiang, N., "Femtosecond Laser Electronic Excitation Tagging Velocimetry in a Transonic, Cryogenic Wind Tunnel," *AIAA Journal* 55(2), 680–685 (2017).
- [17] Chen, L., Yin, Y. M., Li, Y. D., Li, M. and Chen, S., "Application of Femtosecond Laser Electronic Excitation Tagging Velocimetry in Supersonic Mixing Layer Flow Measurement," *Journal of Optics and Precision Engineering* 31(19), 2781–2788 (2023).
- [18] Hill, J. L., Hsu, P. S., Jiang, N., Grib, S. W., Roy, S., Borg, M., Thomas, L., Reeder, M. and Schumaker, S. A., "Hypersonic N₂ boundary layer flow velocity profile measurements using FLEET," *Applied optics* 60(15), C38–C46 (2021).
- [19] Dogariu, L. E., Dogariu, A., Miles, R. B., Smith, M. S. and Marineau, E. C., "Non-Intrusive Hypersonic Freestream and Turbulent Boundary-Layer Velocity Measurements in AEDC Tunnel 9 Using FLEET," (2018).
- [20] Pehrson, J. C., Leonov, B. S., Miles, R. B., Lakebrink, M. T. and Limbach, C., "Wall-normal FLEET Velocimetry in a Canonical Hypersonic Inlet," (2023).
- [21] Peters, C. J., Danehy, P. M., Bathel, B. F., Jiang, N., Calvert, N. and Miles, R. B., "Precision of FLEET Velocimetry using High-Speed CMOS Camera Systems," (2015).
- [22] Chin, S. L., [Femtosecond Laser Filamentation], Springer New York, New York, NY (2010).
- [23] Ryabtsev, A., Pouya, S., Koochesfahani, M. and Dantus, M., "Vortices in the wake of a femtosecond laser filament," *Optics express* 22(21), 26098–26102 (2014).
- [24] Gopal, V., Palmquist, D., Maddalena, L., Dogariu, L. E. and Dogariu, A., "FLEET velocimetry measurements in the ONR-UTA arc-jet wind tunnel," *Exp Fluids* 62(10), 1–17 (2021).
- [25] Zhao, W., Jiang, Z. L., Saito, T., Lin, J. M., Yu, H. R. and Takayama, K., "Performance of a detonation driven shock tunnel," *Shock Waves* 14(1-2), 53–59 (2005).
- [26] Wang, Q., Zhao, W., Teng, H. H. and Jiang, Z. L., "Study on the Non-equilibrium Characteristics of the Flow Field in the High Enthalpy Shock Wind Tunnel Nozzle," *Journal of Aerodynamics* 33(01), 66–71 (2015).
- [27] Dogariu, L. E., Dogariu, A., Miles, R. B., Smith, M. S. and Marineau, E. C., "Femtosecond Laser Electronic Excitation Tagging Velocimetry in a Large-Scale Hypersonic Facility," *AIAA Journal* 57(11), 4725–4737 (2019).